

# Whole-Body Distribution and Radiation Dosimetry of $^{68}\text{Ga}$ -NOTA-RGD, a Positron Emission Tomography Agent for Angiogenesis Imaging

Joong Hyun Kim,<sup>1-3</sup> Jae Sung Lee,<sup>1-5</sup> Keon Wook Kang,<sup>1,3,6</sup> Ho-Young Lee,<sup>1</sup> Sae-Won Han,<sup>7</sup> Tae-You Kim,<sup>7,8</sup> Yun-Sang Lee,<sup>1,3</sup> Jae Min Jeong,<sup>1-3</sup> and Dong Soo Lee<sup>1-3,8</sup>

## Abstract

$^{68}\text{Ga}$  labeled NOTA-RGD was a recently developed positron emission tomography (PET) radiotracer for the visualization of angiogenesis, and is regarded as a promising imaging agent for cancer and several other disorders. In this study, we investigated the whole-body distribution and radiation dosimetry of  $^{68}\text{Ga}$ -NOTA-RGD in humans. Ten cancer patients ( $53.7 \pm 13.5$  years;  $61.5 \pm 7.4$  kg) participated in this study. PET scans were performed using a PET/computed tomography (scanner in three-dimensional mode). After an intravenous injection of  $172.4 \pm 20.5$  MBq of  $^{68}\text{Ga}$ -NOTA-RGD, eight serial whole-body scans were performed during 90 minutes. Volumes of interest were drawn manually over the entire volumes of the urinary bladder, the gallbladder, heart, kidneys, liver, lungs, pancreas, spleen, and stomach. Time-activity curves were obtained from serial PET scan data. Residence times were calculated from areas under curve of time-activity curves and used as input to the OLINDA/EXM 1.1 software. The uptake of  $^{68}\text{Ga}$ -NOTA-RGD was highest in the kidneys and urinary bladder. Radiation doses to kidneys and urinary bladder were  $71.6 \pm 28.4$   $\mu\text{Gy}/\text{MBq}$  and  $239.6 \pm 56.6$   $\mu\text{Gy}/\text{MBq}$ . Mean effective doses were  $25.0 \pm 4.4$   $\mu\text{Sv}/\text{MBq}$  using International Commission of Radiation Protection (ICRP) publication 60 and  $22.4 \pm 3.8$   $\mu\text{Sv}/\text{MBq}$  using ICRP publication 103 weighting factor. We evaluated the radiation dosimetry of  $^{68}\text{Ga}$  labeled NOTA-RGD, which has an acceptable effective radiation dose.

**Key words:** angiogenesis, biodistribution, dosimetry, PET, RGD

## Introduction

Angiogenesis is the physiological process involving the growth of new blood vessels, and an essential developmental process. It is regulated by the interplay of growth factors and inhibitors, and their imbalances can lead to disease. Therefore, the regulation of angiogenesis offers a strategy for the treatment of cancer and other disorders, and

intensive efforts have been undertaken to develop such therapeutic strategies.<sup>1-3</sup>

The integrins are a family of cell-surface receptors that bind extracellular matrix components, organize the cytoskeleton, and activate intracellular signaling pathways.<sup>4</sup> Integrin  $\alpha_v\beta_3$  is a member of this family of receptors, highly expressed on activated endothelial cells during angiogenesis, and associated with the tumor growth, invasion, and metastasis.<sup>5-7</sup>

<sup>1</sup>Department of Nuclear Medicine, Seoul National University College of Medicine, Seoul, Korea.

<sup>2</sup>Interdisciplinary Program in Radiation Applied Life Science, Seoul National University College of Medicine, Seoul, Korea.

<sup>3</sup>Institute of Radiation Medicine, Medical Research Center, Seoul National University College of Medicine, Seoul, Korea.

Departments of <sup>4</sup>WCU Brain and Cognitive Sciences and <sup>5</sup>Biomedical Sciences, Seoul National University College of Medicine, Seoul, Korea.

<sup>6</sup>Cancer Research Institute, Seoul National University College of Medicine, Seoul, Korea.

<sup>7</sup>Department of Internal Medicine, Seoul National University College of Medicine, Seoul, Korea.

<sup>8</sup>WCU Molecular Medicine & Biopharmaceutical Science, Seoul National University College of Medicine, Seoul, Korea.

Address correspondence to: Jae Sung Lee; Department of Nuclear Medicine, Seoul National University College of Medicine; 28 Yungun-Dong, Chongno-Gu, Seoul 110-744, Korea

E-mail: jaes@snu.ac.kr

Keon Wook Kang; Department of Nuclear Medicine, Seoul National University College of Medicine, 101 Daehak-Ro, Jongno-Gu, Seoul 110-744, Korea

E-mail: kangkw@snu.ac.kr

For the targeting of  $\alpha_v\beta_3$ , Arg-Gly-Asp (RGD) derivatives labeled with various radioisotopes, such as,  $^{125}\text{I}$ ,  $^{99\text{m}}\text{Tc}$ ,  $^{18}\text{F}$ ,  $^{90}\text{Y}$ ,  $^{111}\text{In}$ , and  $^{64}\text{Cu}$ , have been developed<sup>8–13</sup> and their biodistribution and dosimetry studies have been examined.<sup>14,15</sup> Recently, 1,4,7-triazacyclononane-1,4,7-triacetic acid (NOTA)-based bifunctional chelating agent was employed to label an RGD peptide to  $^{68}\text{Ga}$ .<sup>16</sup> The importance of  $^{68}\text{Ga}$  for clinical positron emission tomography (PET) imaging has increased recently, because it has several inherent advantages for positron imaging in humans.<sup>17,18</sup> The 67.6 minutes half-life of  $^{68}\text{Ga}$  is suitable for PET imaging, and expected radiation dose is lower than those of other radioisotopes with a longer half-life. High positron yield (89%) and easy accessibility by use of in-house  $^{68}\text{Ge}/^{68}\text{Ga}$  generators are also beneficial physical characteristics.<sup>19</sup> Furthermore, the long half-life (270.8 days) of the parent nuclide  $^{68}\text{Ge}$  allows generators to be used for more than a year.

Human radiation dose evaluation of a new radiotracer is important for risk-benefit assessments in clinical application. The aim of this study was to evaluate the whole-body distribution and radiation dosimetry of  $^{68}\text{Ga}$  labeled NOTA-RGD in humans using biodistribution data obtained by a PET/computed tomography (CT) scanner.

## Materials and Methods

### Radiochemistry

The radiotracer,  $^{68}\text{Ga}$ -NOTA-RGD was synthesized using a minor modification of a previously reported method.<sup>16</sup> Briefly, a NOTA-RGD kit, which contains NOTA-RGD (10.7  $\mu\text{g}$ , 10 nmol), sodium acetate (49.0  $\mu\text{g}$ , 0.6 mmol), and acetic acid (1.8 mg, 29  $\mu\text{mol}$ ), was prepared and used for  $^{68}\text{Ga}$  labeling. Freshly eluted  $^{68}\text{GaCl}_3$  (1.0 mL,  $\sim 740$  MBq/0.1 M HCl solution) solution from a  $^{68}\text{Ge}/^{68}\text{Ga}$ -generator was added to the NOTA-RGD kit using a 24 gauge I.V. catheter and a fluorinated ethylene propylene needle to avoid metal contamination. The reaction mixture was mixed vigorously, and kept at 90°C–95°C for 5 minutes. After the reaction, the reaction mixture was passed through an Alumina N light Sep-Pak<sup>®</sup> cartridge (Waters), which was preconditioned with water (5 mL) and a syringe filter (0.2  $\mu\text{m}$  Supor<sup>®</sup> Membrane Low protein binding; PALL Co.).  $^{68}\text{Ga}$ -NOTA-RGD was eluted with isotonic saline (2 mL). Radiochemical yields and purities were checked by radio-TLC; radiochemical yields were >98% after the  $^{68}\text{Ga}$  labeling procedure, and radiochemical purities were >99.5% after purification.

### Subjects

All procedures of this study were approved by the Institutional Review Board of Seoul National University Hospital, Seoul, Korea. Ten patients (4 women and 6 men) with lung cancer or lymphoma were enrolled in this study. Mean patient age and weight were  $53.7 \pm 13.5$  years (range: 31–72 years) and  $61.5 \pm 7.4$  kg (range: 49–73 kg), respectively.

### PET/CT procedure

A Biograph TruePoint TrueV PET/CT scanner (Siemens Medical) was used in this study to acquire serial emission and transmission scan data sets. The scanner was composed of 4 rings of detector blocks. Each ring contained 48 detector blocks, and each detector block consisted of a  $13 \times 13$  array of

lutetium oxyorthosilicate scintillation crystals, which has a dimension of  $4 \times 4 \times 20$  mm<sup>3</sup>. The axial field-of-view of the PET scanner was 216 mm. The scanner was operated only in the three-dimensional (3D) mode for PET emission scans.

In all patients, the upper body from the neck to the upper thigh was covered by a 5-bed emission scan. To obtain the time-activity curves of organs, eight serial emission scans were performed on all patients over 1.5 hours (about 1.3 times the half-life of  $^{68}\text{Ga}$ ) after an intravenous injection of  $^{68}\text{Ga}$ -NOTA-RGD ( $172.4 \pm 20.5$  MBq). The durations of emission scans varied from 30 to 300 seconds per bed (30, 30, 30, 45, 60, 180, 180, and 300 sec/bed). Scans were started at 1, 4, 7, 10, 15, 30, 46, and 62 minutes postinjection. All patients voided urine after the fifth emission scan to reduce urinary bladder dose. X-ray CT transmission scans were performed twice, before the first and sixth emission scans, to correct for  $\gamma$  ray attenuation and to obtain the anatomical data required for drawing volumes of interest (VOI). The second CT scan was required, because we could not guarantee patient position after voiding is identical with before voiding.

All emission data were reconstructed using the 2D OSEM algorithm with four iterations and eight subsets after random, scatter, attenuation, and normalization corrections and data re-binning. Reconstructed images had dimensions of  $256 \times 256 \times 165$  with 2.67 mm transaxial pixel spacing and 5 mm axial slice interval.

The calibration factor required to convert pixel count rate on emission PET image to activity per volume (MBq/cc) was determined from a  $^{68}\text{Ge}/^{68}\text{Ga}$  phantom study.

### Data analysis

The VOIs of the nine different organs (gall bladder, heart, kidneys, liver, lungs, pancreas, spleen, stomach, and urinary bladder) were drawn to obtain their time-activity curves. VOIs were drawn on CT images for volume invariant organs (gallbladder, heart, kidneys, liver, lungs, pancreas, spleen, and stomach). VOIs drawn on CT images were transferred to eight serial PET emission images, and time-activity curves were obtained. However, since the volume of the urinary bladder increased with time, its VOI was drawn directly on emission PET images.

VOIs were drawn over entire organ volumes.<sup>20,21</sup> The mean activity per unit volume of sub-sampled VOI was not applied in this study, because average subject weight was significantly lower than the standard adult male and female model (73.7 and 56.9 kg) in OLINDA/EXM software (version 1.1, Vanderbilt University, 2007), which was used for dose calculation.<sup>21,22</sup> Furthermore, subject organ volumes were not identical with those of standard phantom models.

Residence times (normalized number of disintegrations) were calculated from time-activity curves. Cumulative activities were obtained by calculating areas under time-activity curves. The area under the curve of each time-activity curve was calculated as the trapezoid sum of observed data and the integral of physical decay for the curve tail after the last scan except the urinary bladder.<sup>23,24</sup> Residence times (hour) were obtained as the ratio of cumulative activity (MBq $\times$ hour) and injected dose to subject (MBq).

Time-activity curves of the urinary bladder showed a pattern unlike that of the other organs. Total urinary bladder activities continuously increased up to the final emission PET

scan (62–87 minutes postinjection). Therefore, the assumption made regarding physical decay of the tail of the curve after the last scan was not appropriate for the urinary bladder, and special modeling of urinary activity was required. The whole-body retention curve of radiotracer was derived from activities in urinary bladder and voiding time (22 and 90 minutes) using dynamic bladder model of Thomas et al.<sup>25</sup> From the whole-body retention curve, time-activity curve and cumulative activity of urinary bladder were estimated.

In addition, the voiding cycle has to be taken into account to calculate residence time for the remainder of the body, because it is also an input parameter of OLINDA/EXM. If voiding urine is prohibited, total residence time ( $RT_{\text{total}}$ ), which is the summation of residence times for all organs and the remainder of body, can be simply calculated using the following equation:

$$RT_{\text{total}} = \frac{\int_0^{\infty} A_0 \times \exp(-\lambda t) dt}{A_0} \approx 1.443 \times T_{1/2}$$

where  $A_0$  is the initial activity of injected dose, and  $\lambda$  is the decay constant of the radioisotope. Total residence time is almost 1.443 times the half-life ( $T_{1/2}$ ) of the radioisotope. On the other hand, if voiding urine is considered, total residence time cannot be obtained using the equation just cited, because excreted activities by voiding have to be subtracted. In this study, voiding excretion (“urine out” in Table 1) was taken into account to calculate residence times for the remainder of the body.

The radiation dose to each organ, effective dose (ED), and effective dose equivalent (EDE) were calculated using individual organ residence times. These variables were also calculated using 1-hour and 1.5-hour voiding models.

#### Effective radiation dose estimation

The residence times obtained using the procedures just mentioned were used as input parameters for OLINDA/EXM 1.1 software. OLINDA/EXM 1.1 reports individual doses for 24–25 target organs and effective radiation doses

(EDE and ED). Effective radiation doses are obtained using weighted sums of individual doses to each target organ. EDE was defined as in International Commission of Radiation Protection (ICRP) publication 26 (1977), and was calculated using weighting factors and doses to six major target organs and five remainder organs. The EDE was revised to ED as defined by ICRP publication 60 (1990), which used revised radiation detriment values and tissue weighting factors. In addition, the ED takes more organs into account than the EDE. Eleven major organs and 10 remainder organs were included to calculate EDE. These 2 effective radiation dose calculations were implemented in OLINDA/EXM 1.1 software.

Recently, new tissue weighting factors were introduced in ICRP publication 103 (2007).<sup>26</sup> In this publication, more organs are considered than in ICRP60, and the weighting factors of two critical organs were changed significantly (gonad 20% → 8%, breast 5% → 12%).

Although the ICRP103-defined ED is not implemented in OLINDA/EXM software, it can be calculated using tissue weighting factors and individual target doses. In this article, 3 types of effective radiation doses were estimated.

## Results

Figure 1 shows the serial emission PET scan data of a patient. High accumulation of <sup>68</sup>Ga-NOTA-RGD was observed on urinary excretion tracks (i.e., kidneys and the urinary bladder). The liver was also found to be a high accumulation organ in all time frames. Activity in the urinary bladder dropped after the 5th emission scan because of urine voiding.

Graphs of percentage of injected dose (%ID) versus time are shown in Figure 2 (uncorrected for radiation decay). As was expected, the %ID of urinary bladder dropped after voiding. Cumulative activity percentages and organ residence times are shown in Table 1, and as expected, high %ID values and residence times were shown for the urinary bladder, kidneys, and liver. The residence time of urinary bladder was much higher than those of other organs, even though a 2-hour voiding model was employed. About 10.8% of injected doses concentrated in the urinary bladder. In tumor lesion, the %ID per unit volume (liter) was comparable to the liver.

The radiation doses absorbed by each organ, EDE by ICRP26, and ED by ICRP60 (all obtained using OLINDA/EXM 1.1 software), and ED by ICRP103 (calculated as the weighted sum of individual doses) are presented in Table 2. High radiation doses were reported for the urinary bladder wall ( $239.6 \pm 56.6 \mu\text{Gy}/\text{MBq}$ ) and kidneys ( $71.6 \pm 28.4 \mu\text{Gy}/\text{MBq}$ ). Mean EDE by ICRP26 and ED by ICRP60 and ICRP103 were  $31.9 \pm 5.4 \mu\text{Sv}/\text{MBq}$ ,  $25.0 \pm 4.4 \mu\text{Sv}/\text{MBq}$ , and  $22.4 \pm 3.8 \mu\text{Sv}/\text{MBq}$ , respectively.

Residence times in urinary bladder, radiation doses to bladder walls, ED, and EDE values at various voiding frequencies after scans are listed in Table 3. More frequent voiding reduced radiation dose. The 1-hour voiding model yielded a 12.9% lower dose to the bladder wall, and a 6.6% lower ED (by ICRP60).

## Discussion

<sup>68</sup>Ga labeled NOTA-RGD was a recently developed radiotracer for PET to visualize angiogenesis, and is a

TABLE 1. CUMULATIVE ACTIVITY PERCENTAGES (%ID), CUMULATIVE ACTIVITY PERCENTAGE PER UNIT VOLUME (%ID/L), AND MEAN RESIDENCE TIMES (HOUR)

Organ	Subject no. <sup>a</sup>	%ID	%ID/L	Residence time ( $\times 100$ , hour)
Gallbladder	8	0.02	1.49	0.03 ± 0.02
Heart	10	1.31	2.08	2.13 ± 0.51
Kidneys	10	2.63	7.87	4.28 ± 1.67
Liver	10	3.65	2.33	5.93 ± 1.12
Lungs	10	2.17	0.81	3.53 ± 0.53
Pancreas	8	0.03	1.87	0.05 ± 0.04
Spleen	10	0.54	2.91	0.88 ± 0.36
Stomach	10	0.57	1.36	0.92 ± 0.24
Urinary bladder	10	10.84	N/A	17.62 ± 3.37
Urine out	10	18.01	N/A	29.29 ± 7.89
Remainder of body	10	60.24	N/A	97.95 ± 11.79
Tumor	5	0.05	2.44	0.09 ± 0.08
Total		100		162.61

<sup>a</sup>Number of patients in whom the organ could be identified. %ID, percentage of injected dose.

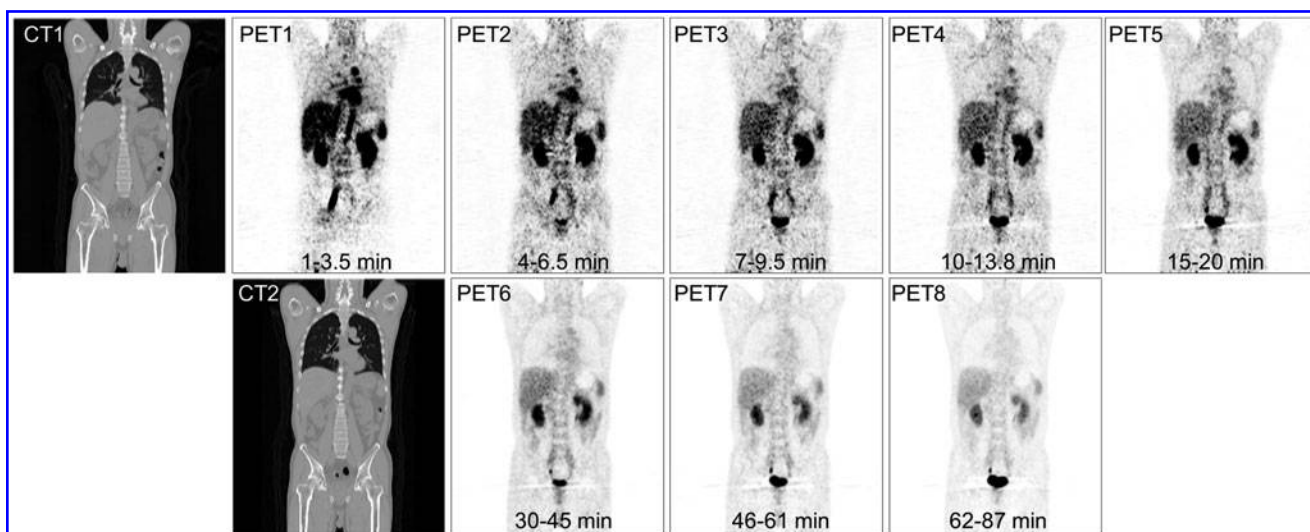


**FIG. 1.** Transmission and emission scan data set of a 49 year-old male subject. Two X-ray CT transmission scans were performed before the 1st and 6th emission PET scans. High accumulation of radiotracer was shown in the urinary bladder, kidneys, and liver. Activity in the urinary bladder dropped after the 5th emission scan because of urine voiding. The injected radiation dose of  $^{68}\text{Ga}$ -NOTA-RGD was 167.4 MBq. CT, computed tomography; PET, positron emission tomography.

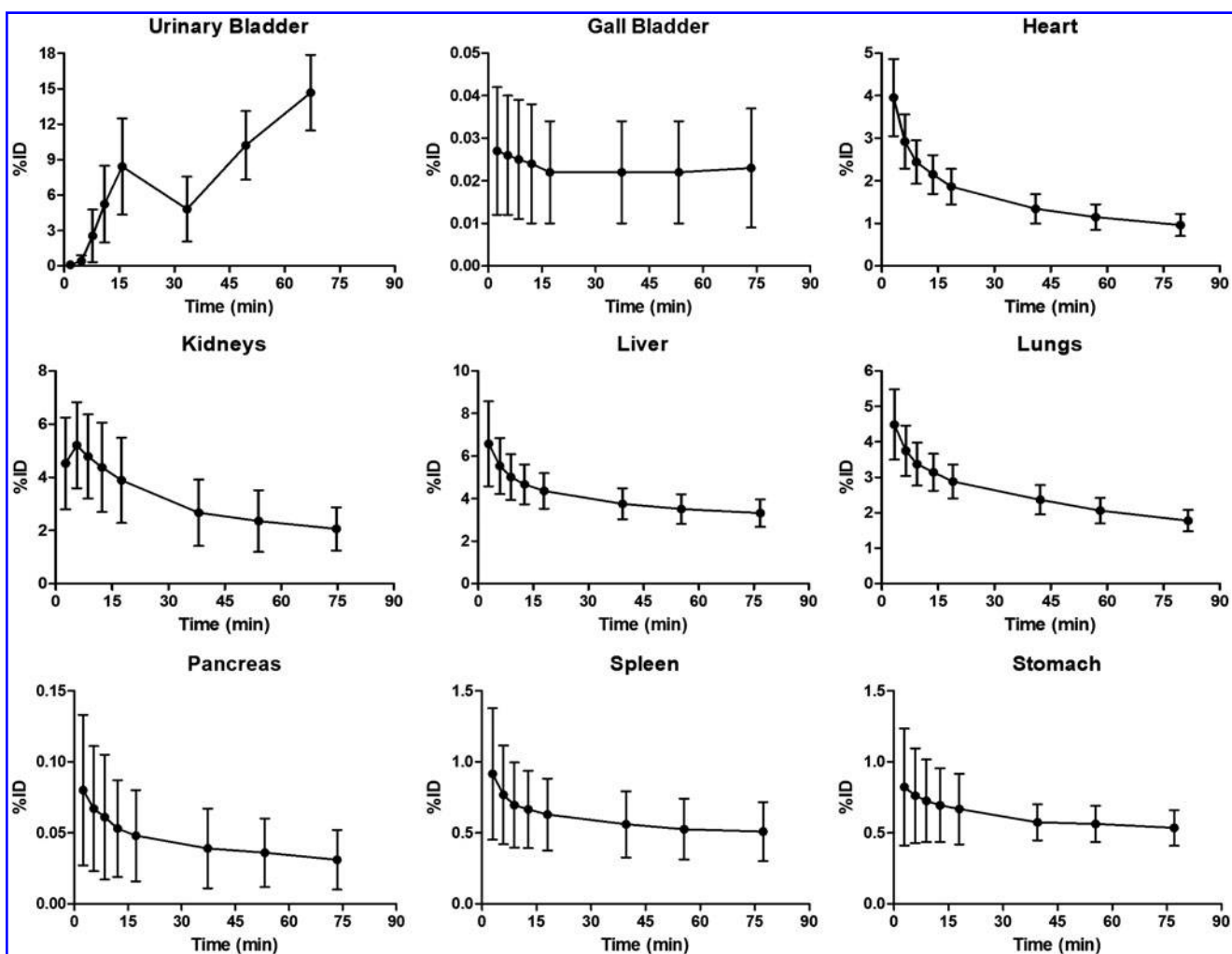


**FIG. 2.** Graphs of percentage injected dose (%ID, mean  $\pm$  SD) versus time for the nine organs (uncorrected for radiation decay). The %ID of the urinary bladder dropped after the 5th scan. Those of all the other organs showed decreasing activity. SD, standard deviation.

TABLE 2. ORGAN RADIATION DOSES, EFFECTIVE DOSES, AND EFFECTIVE DOSE EQUIVALENTS

Organ	Radiation dose ( $\mu\text{Gy}/\text{MBq}$ )
Adrenals	11.76 $\pm$ 2.24
Brain	8.96 $\pm$ 1.90
Breasts	9.02 $\pm$ 1.86
Gallbladder wall	12.72 $\pm$ 2.37
Lower large intestine wall	12.98 $\pm$ 2.25
Small intestine	11.60 $\pm$ 1.92
Stomach wall	18.26 $\pm$ 4.27
Upper large intestine wall	11.55 $\pm$ 2.20
Heart wall	22.29 $\pm$ 4.62
Kidneys	71.61 $\pm$ 28.38
Liver	20.87 $\pm$ 4.21
Lungs	20.89 $\pm$ 4.62
Muscle	10.26 $\pm$ 1.93
Ovaries	12.99 $\pm$ 2.25
Pancreas	8.97 $\pm$ 3.08
Red marrow	8.51 $\pm$ 1.48
Osteogenic cells	14.46 $\pm$ 3.42
Skin	8.71 $\pm$ 1.73
Spleen	27.52 $\pm$ 7.92
Testes ( $n=6$ )	9.63 $\pm$ 0.66
Thymus	10.26 $\pm$ 2.11
Thyroid	9.53 $\pm$ 1.80
Urinary bladder wall	239.60 $\pm$ 56.58
Uterus	15.82 $\pm$ 2.11
Total body	11.39 $\pm$ 2.03
EDE ( $\mu\text{Sv}/\text{MBq}$ ) by ICRP26	31.86 $\pm$ 5.41
ED ( $\mu\text{Sv}/\text{MBq}$ ) by ICRP60	24.98 $\pm$ 4.39
ED ( $\mu\text{Sv}/\text{MBq}$ ) by ICRP103	22.37 $\pm$ 3.84

ED, effective dose; EDE, effective dose equivalent; ICRP, International Commission of Radiation Protection.

promising candidate for cancer imaging.<sup>8,16,18</sup> The aim of this study was to evaluate radiation dose exposure to humans who undergo a <sup>68</sup>Ga-NOTA-RGD emission PET scan. In this study, radiation dosimetry of <sup>68</sup>Ga-NOTA-RGD was examined in 10 human subjects who underwent eight serial emission PET scans of the upper body from the neck to the upper thigh to obtain the time-activity curves of nine anatomic organs. Absorbed doses were estimated using OLINDA/EXM 1.1 software.

In the present study, the predominance of renal excretion of <sup>68</sup>Ga-NOTA-RGD observed in mice<sup>16</sup> was also confirmed in humans (Fig. 1). Activities in urinary bladder dropped considerably after voiding urine, which usefully reduced dose to the urinary bladder wall. The 6th scan data acquired after voiding was found to be useful for highlighting tumor regions because of the reduced urinary bladder activity.

Although a 2-hour voiding model was primarily employed in this study to estimate residence time in the urinary bladder contents, our results (Table 3) also showed that more frequent voiding, such as, 1- or 1.5-hour voiding, helpfully reduced urinary bladder activity and radiation dose. Accordingly, frequent urine voiding is recommended to patients who undergo a PET scan with <sup>68</sup>Ga-NOTA-RGD.

The activities in urinary bladder contents were found to be increasing at the end of our study ( $\sim 90$  minutes). However, the time-activity curve of the urinary bladder could be derived using the dynamic bladder model of Thomas et al.<sup>25</sup> This model was useful to estimate excreted activities by voiding and residence time for the remainder of the body.

In a previous study, the whole-body distribution and radiation dosimetry of <sup>18</sup>F-galacto-RGD was performed in human subjects, which also shows rapid clearance, primarily via the renal pathway.<sup>14</sup> The ED and dose to the urinary bladder wall of <sup>18</sup>F-galacto-RGD were 18.7  $\mu\text{Sv}/\text{MBq}$  and 220  $\mu\text{Gy}/\text{MBq}$ , respectively. In the present study, <sup>68</sup>Ga-NOTA-RGD showed equivalent to or slightly higher radiation dose than <sup>18</sup>F-galacto-RGD (Tables 2 and 3). Although <sup>68</sup>Ga-labeled radiotracers have considerably shorter physical half-lives than <sup>18</sup>F-labeled radiotracers (67.63 vs. 109.8 minutes), this difference is balanced in terms of the radiation dose by the initial kinetic energy of positrons emitted ( $E_{\text{max}}=1899$  keV for <sup>68</sup>Ga vs. 633 keV for <sup>18</sup>F). However, it should be noted that different internal distributions of these radiotracers is another determinant factor of the radiation dose.

The ED values of other PET radiotracers recently reported in the literature are listed in Table 4, which shows that the ED of <sup>68</sup>Ga-NOTA-RGD is comparable to those of other <sup>68</sup>Ga-labeled radiotracers.<sup>14,15,26-34</sup> The ED values of <sup>68</sup>Ga-labeled radiotracers lie between those of <sup>11</sup>C-labeled and <sup>18</sup>F-labeled radiotracers. <sup>11</sup>C-labeled radiotracers have significantly lower doses than <sup>68</sup>Ga- and <sup>18</sup>F-labeled radiotracers, due to the much shorter half-life of <sup>11</sup>C (20.4 minutes). On the other hand, the ED difference between <sup>68</sup>Ga- and <sup>18</sup>F-labeled radiotracers is not large because of the balance between half-life and positron energy just mentioned.

In this study, ED by ICRP publication 103 was calculated using the weighted sums of individual organ doses, and compared with ED by ICRP60. Renal excretion is a predominant feature for <sup>68</sup>Ga-NOTA-RGD; therefore, the radiation dose to the urinary bladder wall was particularly high. The tissue weighting factor for the urinary bladder wall decreased from 5% for ICRP60 to 4% for ICRP103. That would be why the ED by ICRP103 was lower than that by ICRP60.

In the present study, we evaluated the radiation dosimetry of <sup>68</sup>Ga labeled NOTA-RGD, which has an acceptable

TABLE 3. RESIDENCE TIMES OF URINARY BLADDER CONTENTS, RADIATION DOSES TO THE URINARY BLADDER WALL, EFFECTIVE DOSE EQUIVALENTS, AND EFFECTIVE DOSES FOR THREE DIFFERENT VOIDING CYCLES

Voiding cycle	2 hours	1.5 hours	1 hour
Residence time of urinary bladder contents ( $\times 100$ , hours)	17.62 $\pm$ 3.37	15.70 $\pm$ 3.22	15.23 $\pm$ 2.93
Radiation dose to urinary bladder wall ( $\mu\text{Gy}/\text{MBq}$ )	239.60 $\pm$ 56.58	214.50 $\pm$ 53.10	208.60 $\pm$ 50.79
EDE ( $\mu\text{Sv}/\text{MBq}$ ) by ICRP26	31.86 $\pm$ 5.41	30.28 $\pm$ 5.17	29.90 $\pm$ 5.10
ED ( $\mu\text{Sv}/\text{MBq}$ ) by ICRP60	24.98 $\pm$ 4.39	23.66 $\pm$ 4.20	23.32 $\pm$ 4.16
ED ( $\mu\text{Sv}/\text{MBq}$ ) by ICRP103	22.37 $\pm$ 3.84	21.29 $\pm$ 3.68	21.04 $\pm$ 3.66

TABLE 4. THE EFFECTIVE RADIATION DOSES OF POSITRON EMISSION TOMOGRAPHY RADIOTRACERS

Radiotracer	Effective dose ( $\mu\text{Sv}/\text{MBq}$ )	Effective dose equivalent ( $\mu\text{Sv}/\text{MBq}$ )	References
$^{68}\text{Ga}$ -DOTA TOC	23		27
$^{68}\text{Ga}$ -DOTA NOC	16.7	25.4	28
$^{68}\text{Ga}$ -NOTA-RGD	25.0/22.4 <sup>a</sup>	31.9	This study
[ $^{11}\text{C}$ ]- (R)-PK11195	4.8/5.1 <sup>a</sup>		26
[ $^{11}\text{C}$ ]PIB	4.2		29
[ $^{11}\text{C}$ ]Acetate	4.9		30
[ $^{11}\text{C}$ ]Raclopride	6.5		31
[ $^{18}\text{F}$ ]FDG	18.9		32
[ $^{18}\text{F}$ ]AV-133	27.8	36.5	33
[ $^{18}\text{F}$ ]GE067	33.8		34
$^{18}\text{F}$ -Galacto-RGD	18.7		14
[ $^{18}\text{F}$ ]AH111585	26		15

<sup>a</sup>According to ICRP103.

effective radiation dose. Furthermore, the ED of  $^{68}\text{Ga}$ -NOTA-RGD was comparable with those of other  $^{68}\text{Ga}$ -labeled tracers.

### Acknowledgments

This work was supported by grants from the Atomic Energy R&D Program (2008-2003852, 2010-0026012) and the World Class University Program (R32-10142) through the Korean Science and Engineering Foundation funded by the Korean Ministry of Education, Science, and Technology and the Korean Healthcare Technology R&D Project (A070001) funded by Ministry of Health and Welfare, Republic of Korea.

### Disclosure Statement

The authors declare that they have no conflict of interest.

### References

1. Veikkola T, Karkkainen M, Claesson-Welsh L, et al. Regulation of angiogenesis via vascular endothelial growth factor receptors. *Cancer Res* 2000;60:203.
2. Carmeliet P. Angiogenesis in life, disease and medicine. *Nature* 2005;438:932.
3. Ferrara N, Kerbel RS. Angiogenesis as a therapeutic target. *Nature* 2005;438:967.
4. Guo W, Giancotti FG. Integrin signalling during tumour progression. *Nat Rev Mol Cell Biol* 2004;5:816.
5. Brooks PC, Montgomery AM, Rosenfeld M, et al. Integrin  $\alpha_v\beta_3$  antagonists promote tumor regression by inducing apoptosis of angiogenic blood vessels. *Cell* 1994;79:1157.
6. Hood JD, Cheresch DA. Role of integrins in cell invasion and migration. *Nat Rev Cancer* 2002;2:91.
7. Ruoslahti E. Specialization of tumour vasculature. *Nat Rev Cancer* 2002;2:83.
8. Haubner R, Beer AJ, Wang H, et al. Positron emission tomography tracers for imaging angiogenesis. *Eur J Nucl Med Mol Imaging* 2010;37(Suppl):S86.
9. Yang J, Guo H, Miao Y. Technetium-99m-labeled Arg-Gly-Asp-conjugated alpha-melanocyte stimulating hormone hybrid peptides for human melanoma imaging. *Nucl Med Biol* 2010;37:873.
10. Yan Y, Chen K, Yang M, et al. A new  $^{18}\text{F}$ -labeled BBN-RGD peptide heterodimer with a symmetric linker for prostate cancer imaging. *Amino Acids* 2011;41:439.
11. Picchio M, Beck R, Haubner R, et al. Intratumoral spatial distribution of hypoxia and angiogenesis assessed by  $^{18}\text{F}$ -FAZA and  $^{125}\text{I}$ -Gluco-RGD autoradiography. *J Nucl Med* 2008;49:597.
12. Liu Z, Yan Y, Liu S, et al.  $^{18}\text{F}$ ,  $^{64}\text{Cu}$ , and  $^{68}\text{Ga}$  labeled RGD-bombesin heterodimeric peptides for PET imaging of breast cancer. *Bioconjug Chem* 2009;20:1016.
13. Yoshimoto M, Ogawa K, Washiyama K, et al.  $\alpha_v\beta_3$  Integrin-targeting radionuclide therapy and imaging with monomeric RGD peptide. *Int J Cancer* 2008;123:709.
14. Beer AJ, Haubner R, Wolf I, et al. PET-based human dosimetry of  $^{18}\text{F}$ -galacto-RGD, a new radiotracer for imaging  $\alpha_v\beta_3$  expression. *J Nucl Med* 2006;47:763.
15. McParland BJ, Miller MP, Spinks TJ, et al. The biodistribution and radiation dosimetry of the Arg-Gly-Asp peptide  $^{18}\text{F}$ -AH111585 in healthy volunteers. *J Nucl Med* 2008;49:1664.
16. Jeong JM, Hong MK, Chang YS, et al. Preparation of a promising angiogenesis PET imaging agent:  $^{68}\text{Ga}$ -labeled c(RGDyK)-isothiocyanatobenzyl-1,4,7-triazacyclononane-1,4,7-triacetic acid and feasibility studies in mice. *J Nucl Med* 2008;49:830.
17. Breeman WA, Verbruggen AM. The  $^{68}\text{Ge}/^{68}\text{Ga}$  generator has high potential, but when can we use  $^{68}\text{Ga}$ -labelled tracers in clinical routine? *Eur J Nucl Med Mol Imaging* 2007;34:978.
18. Shetty D, Lee YS, Jeong JM.  $^{68}\text{Ga}$ -labeled radiopharmaceuticals for positron emission tomography. *Nucl Med Mol Imaging* 2010;44:233.
19. Ehrhardt GJ, Welch MJ. A new germanium-68/gallium-68 generator. *J Nucl Med* 1978;19:925.
20. Kolbert KS, Pentlow KS, Pearson JR, et al. Prediction of absorbed dose to normal organs in thyroid cancer patients treated with  $^{131}\text{I}$  by use of  $^{124}\text{I}$  PET and 3-dimensional internal dosimetry software. *J Nucl Med* 2007;48:143.
21. Antenor-Dorsey JA, Laforest R, Moerlein SM, et al. Radiation dosimetry of N-([ $^{11}\text{C}$ ]methyl)benperidol as determined by whole-body PET imaging of primates. *Eur J Nucl Med Mol Imaging* 2008;35:771.
22. Stabin MG, Sparks RB, Crowe E. OLINDA/EXM: The second-generation personal computer software for internal dose assessment in nuclear medicine. *J Nucl Med* 2005;46:1023.
23. Treyer V, Streffer J, Ametamey SM, et al. Radiation dosimetry and biodistribution of  $^{11}\text{C}$ -ABP688 measured in healthy volunteers. *Eur J Nucl Med Mol Imaging* 2008;35:766.
24. Nye JA, Schuster DM, Yu W, et al. Biodistribution and radiation dosimetry of the synthetic nonmetabolized amino acid analogue anti- $^{18}\text{F}$ -FACBC in humans. *J Nucl Med* 2007;48:1017.
25. Thomas SR, Stabin MG, Chen CT, et al. MIRD Pamphlet No. 14 revised: A dynamic urinary bladder model for radiation dose calculations. *J Nucl Med* 1999;40:1025.
26. Hirvonen J, Roivainen A, Virta J, et al. Human biodistribution and radiation dosimetry of  $^{11}\text{C}$ -(R)-PK11195, the prototypic PET ligand to image inflammation. *Eur J Nucl Med Mol Imaging* 2010;37:606.
27. Hartmann H, Zöphel K, Freudenberg R, et al. Radiation exposure of patients during  $^{68}\text{Ga}$ -DOTATOC PET/CT examinations. *Nuklearmedizin* 2009;48:201.

28. Pettinato C, Sarnelli A, Di Donna M, et al.  $^{68}\text{Ga}$ -DOTANOC: Biodistribution and dosimetry in patients affected by neuroendocrine tumors. *Eur J Nucl Med Mol Imaging* 2008; 35:72.
29. Scheinin NM, Tolvanen TK, Wilson IA, et al. Biodistribution and radiation dosimetry of the amyloid imaging agent  $^{11}\text{C}$ -PIB in humans. *J Nucl Med* 2007;48:128.
30. Seltzer MA, Jahan SA, Sparks R, et al. Radiation dose estimates in humans for  $^{11}\text{C}$ -acetate whole-body PET. *J Nucl Med* 2004;45:1233.
31. Slifstein M, Hwang DR, Martinez D, et al. Biodistribution and radiation dosimetry of the dopamine  $\text{D}_2$  ligand  $^{11}\text{C}$ -raclopride determined from human whole-body PET. *J Nucl Med* 2006;47:313.
32. Leide-Svegborn S. Radiation exposure of patients and personnel from a PET/CT procedure with  $^{18}\text{F}$ -FDG. *Radiat Prot Dosimetry* 2010;139:208.
33. Lin KJ, Weng YH, Wey SP, et al. Whole-body biodistribution and radiation dosimetry of  $^{18}\text{F}$ -FP-(+)-DTBZ ( $^{18}\text{F}$ -AV-133): A novel vesicular monoamine transporter 2 imaging agent. *J Nucl Med* 2010;51:1480.
34. Koole M, Lewis DM, Buckley C, et al. Whole-body biodistribution and radiation dosimetry of  $^{18}\text{F}$ -GE067: A radioligand for *in vivo* brain amyloid imaging. *J Nucl Med* 2009;50:818.

This article has been cited by:

1. Olli Moisio, Senthil Palani, Jenni Virta, Petri Elo, Heidi Liljenbäck, Tuula Tolvanen, Meeri Käkälä, Maxwell G. Miner, Erika Atencio Herre, Päivi Marjamäki, Tiit Örd, Merja Heinäniemi, Minna U. Kaikkonen, Fenghua Zhang, Madduri Srinivasarao, Juhani Knuuti, Philip S. Low, Antti Saraste, Xiang-Guo Li, Anne Roivainen. 2020. Radiosynthesis and preclinical evaluation of [<sup>68</sup>Ga]Ga-NOTA-folate for PET imaging of folate receptor  $\beta$ -positive macrophages. *Scientific Reports* 10:1. . [[Crossref](#)]
2. Thomas Ebenhan, Janke Kleynhans, Jan Rijn Zeevaart, Jae Min Jeong, Mike Sathekge. 2020. Non-oncological applications of RGD-based single-photon emission tomography and positron emission tomography agents. *European Journal of Nuclear Medicine and Molecular Imaging* 2. . [[Crossref](#)]
3. Farshad Moradi, Andrei Iagaru. 2020. The Role of Positron Emission Tomography in Pancreatic Cancer and Gallbladder Cancer. *Seminars in Nuclear Medicine* 50:5, 434-446. [[Crossref](#)]
4. Min Sun Lee, Donghwi Hwang, Joong Hyun Kim, Jae Sung Lee. 2019. Deep-dose: a voxel dose estimation method using deep convolutional neural network for personalized internal dosimetry. *Scientific Reports* 9:1. . [[Crossref](#)]
5. Vatsa Rakhee, Shukla Jaya, Kumar Sunil, Chakraborty Sudipta, Dash Ashutosh, Singh Gurpreet, Mittal Bhagwant Rai. 2019. Effect of Macro-Cyclic Bifunctional Chelators DOTA and NODAGA on Radiolabeling and In Vivo Biodistribution of Ga-68 Cyclic RGD Dimer. *Cancer Biotherapy & Radiopharmaceuticals* 34:7, 427-435. [[Abstract](#)] [[Full Text](#)] [[PDF](#)] [[PDF Plus](#)]
6. Junwoo Kim, Chang-Ock Lee. 2019. Three-Dimensional Volume Reconstruction Using Two-Dimensional Parallel Slices. *SIAM Journal on Imaging Sciences* 12:1, 1-27. [[Crossref](#)]
7. Frederic Debordeaux, Lucie Chansel-Debordeaux, Jean-Baptiste Pinaquy, Philippe Fernandez, Jurgen Schulz. 2018. What about  $\alpha v\beta 3$  integrins in molecular imaging in oncology?. *Nuclear Medicine and Biology* 62-63, 31-46. [[Crossref](#)]
8. Soomin Jeon, Chang-Ock Lee. 2018. A CT metal artifact reduction algorithm based on sinogram surgery. *Journal of X-Ray Science and Technology* 26:3, 413-434. [[Crossref](#)]
9. Jothilingam Sivapackiam, Richard Laforest, Vijay Sharma. 2018. <sup>68</sup>Ga[Ga]-Galmydar: Biodistribution and radiation dosimetry studies in rodents. *Nuclear Medicine and Biology* 59, 29-35. [[Crossref](#)]
10. Silvano Gnesin, Periklis Mitsakis, Francesco Cicone, Emmanuel Deshayes, Vincent Dunet, Augusto F. Gallino, Marek Kosinski, Sébastien Baechler, Franz Buchegger, David Viertl, John O. Prior. 2017. First in-human radiation dosimetry of <sup>68</sup>Ga-NODAGA-RGDyK. *EJNMMI Research* 7:1. . [[Crossref](#)]
11. Markus Nieberler, Ute Reuning, Florian Reichart, Johannes Notni, Hans-Jürgen Wester, Markus Schwaiger, Michael Weinmüller, Andreas Räder, Katja Steiger, Horst Kessler. 2017. Exploring the Role of RGD-Recognizing Integrins in Cancer. *Cancers* 9:12, 116. [[Crossref](#)]
12. Shi Shu, Li Zhang, Yi Cheng Zhu, Fang Li, Li Ying Cui, Hao Wang, Yi Sun, Pei Lin Wu, Zhao Hui Zhu, Bin Peng. 2017. Imaging angiogenesis using <sup>68</sup>Ga-NOTA-PRGD2 positron emission tomography/computed tomography in patients with severe intracranial atherosclerotic disease. *Journal of Cerebral Blood Flow & Metabolism* 37:10, 3401-3408. [[Crossref](#)]
13. Isaac M. Jackson, Peter J.H. Scott, Stephen Thompson. 2017. Clinical Applications of Radiolabeled Peptides for PET. *Seminars in Nuclear Medicine* 47:5, 493-523. [[Crossref](#)]
14. Fei Kang, Zhe Wang, Guoquan Li, Shengjun Wang, Daliang Liu, Mingru Zhang, Mingxuan Zhao, Weidong Yang, Jing Wang. 2017. Inter-heterogeneity and intra-heterogeneity of  $\alpha v\beta 3$  in non-small cell lung cancer and small cell lung cancer patients as revealed by <sup>68</sup>Ga-RGD2 PET imaging. *European Journal of Nuclear Medicine and Molecular Imaging* 44:9, 1520-1528. [[Crossref](#)]
15. Thomas Ebenhan, Isabel Schoeman, Daniel D. Rossouw, Anne Grobler, Biljana Marjanovic-Painter, Judith Wagener, Hendrik G. Kruger, Mike M. Sathekge, Jan Rijn Zeevaart. 2017. Evaluation of a Flexible NOTA-RGD Kit Solution Using Gallium-68 from Different <sup>68</sup>Ge/<sup>68</sup>Ga-Generators: Pharmacokinetics and Biodistribution in Nonhuman Primates and Demonstration of Solitary Pulmonary Nodule Imaging in Humans. *Molecular Imaging and Biology* 19:3, 469-482. [[Crossref](#)]
16. Katharina A. Domnanich, Cristina Müller, Renata Farkas, Raffaella M. Schmid, Bernard Ponsard, Roger Schibli, Andreas Türlér, Nicholas P. van der Meulen. 2017. <sup>44</sup>Sc for labeling of DOTA- and NODAGA-functionalized peptides: preclinical in vitro and in vivo investigations. *EJNMMI Radiopharmacy and Chemistry* 1:1. . [[Crossref](#)]
17. Didier J. Colin, James A. H. Inkster, Stéphane Germain, Yann Seimille. 2017. Preclinical validations of [<sup>18</sup>F]FPyPEGCBT-c(RGDfK): a <sup>18</sup>F-labelled RGD peptide prepared by ligation of 2-cyanobenzothiazole and 1,2-aminothiol to image angiogenesis. *EJNMMI Radiopharmacy and Chemistry* 1:1. . [[Crossref](#)]
18. Zhang Zhaoqi, Zhao Xinming, Ding Cuimin, Wang Jianfang, Zhang Jingmian, Wang Fan. 2016. <sup>99m</sup>Tc-3PRGD2 SPECT/CT Imaging for Monitoring Early Response of EGFR-TKIs Therapy in Patients with Advanced-Stage Lung Adenocarcinoma. *Cancer Biotherapy & Radiopharmaceuticals* 31:7, 238-245. [[Abstract](#)] [[Full Text](#)] [[PDF](#)] [[PDF Plus](#)]

19. Jae Seon Eo, Jae Min Jeong. 2016. Angiogenesis Imaging Using 68Ga-RGD PET/CT: Therapeutic Implications. *Seminars in Nuclear Medicine* **46**:5, 419-427. [[Crossref](#)]
20. Teresa A. Szyszko, Connie Yip, Peter Szlosarek, Vicky Goh, Gary J.R. Cook. 2016. The role of new PET tracers for lung cancer. *Lung Cancer* **94**, 7-14. [[Crossref](#)]
21. Raisa N. Krasikova, Ramiz A. Aliev, Stepan N. Kalmykov. 2016. The next generation of positron emission tomography radiopharmaceuticals labeled with non-conventional radionuclides. *Mendeleev Communications* **26**:2, 85-94. [[Crossref](#)]
22. Ryogo Minamimoto, Mehran Jamali, Amir Barkhodari, Camila Mosci, Erik Mittra, Bin Shen, Frederick Chin, Sanjiv Sam Gambhir, Andrei Iagaru. 2015. Biodistribution of the 18F-FPPRGD2 PET radiopharmaceutical in cancer patients: an atlas of SUV measurements. *European Journal of Nuclear Medicine and Molecular Imaging* **42**:12, 1850-1858. [[Crossref](#)]
23. Young Sub Lee, Jin Su Kim, Kyung Deuk Cho, Joo Hyun Kang, Sang Moo Lim. 2015. Tumor dosimetry for I-131 trastuzumab therapy in a Her2+ NCI N87 xenograft mouse model using the Siemens SYMBIA E gamma camera with a pinhole collimator. *Journal of Instrumentation* **10**:07, P07001-P07001. [[Crossref](#)]
24. Jae Seon Eo, Hyun Koo Kim, Sungeun Kim, Yun-Sang Lee, Jae Min Jeong, Young Ho Choi. 2015. Gallium-68 Neomannosylated Human Serum Albumin-Based PET/CT Lymphoscintigraphy for Sentinel Lymph Node Mapping in Non-small Cell Lung Cancer. *Annals of Surgical Oncology* **22**:2, 636-641. [[Crossref](#)]
25. Hai-Jeon Yoon, Keon Wook Kang, In Kook Chun, Nariya Cho, Seock-Ah Im, Sunjoo Jeong, Song Lee, Kyeong Cheon Jung, Yun-Sang Lee, Jae Min Jeong, Dong Soo Lee, June-Key Chung, Woo Kyung Moon. 2014. Correlation of breast cancer subtypes, based on estrogen receptor, progesterone receptor, and HER2, with functional imaging parameters from 68Ga-RGD PET/CT and 18F-FDG PET/CT. *European Journal of Nuclear Medicine and Molecular Imaging* **41**:8, 1534-1543. [[Crossref](#)]
26. Roland Haubner, Simone Maschauer, Olaf Prante. 2014. PET Radiopharmaceuticals for Imaging Integrin Expression: Tracers in Clinical Studies and Recent Developments. *BioMed Research International* **2014**, 1-17. [[Crossref](#)]
27. Joseph M. Herman, Lauren M. Rosati, Timothy M. Pawlik, Charles R. Thomas. Future Directions 333-338. [[Crossref](#)]
28. Joong Hyun Kim, Young-Hwa Kim, Young Joo Kim, Bo Yeun Yang, Jae Min Jeong, Hyewon Youn, Dong Soo Lee, Jae Sung Lee. 2013. Quantitative positron emission tomography imaging of angiogenesis in rats with forelimb ischemia using 68Ga-NOTA-c(RGDyK). *Angiogenesis* **16**:4, 837-846. [[Crossref](#)]
29. Erik H. J. G. Aarntzen, Mangala Srinivas, Caius G. Radu, Cornelis J. A. Punt, Otto C. Boerman, Carl G. Figdor, Wim J. G. Oyen, I. Jolanda M. de Vries. 2013. In vivo imaging of therapy-induced anti-cancer immune responses in humans. *Cellular and Molecular Life Sciences* **70**:13, 2237-2257. [[Crossref](#)]
30. E. Deshayes, V. Dunet, C. Rüegg, J.O. Prior. 2012. Imagerie de la néoangiogenèse en médecine nucléaire. *Médecine Nucléaire* **36**:10, 619-626. [[Crossref](#)]
31. Jeffrey T. Gu, Linda Nguyen, Abhijit J. Chaudhari, John D. MacKenzie. 2011. Molecular Characterization of Rheumatoid Arthritis With Magnetic Resonance Imaging. *Topics in Magnetic Resonance Imaging* **22**:2, 61-69. [[Crossref](#)]